Hydrocyclone Separation Efficiency Modeled by Flow Resistances and Droplet Trajectories

Mads Valentin Bram * **Leif Hansen** * **Dennis Severin Hansen** * **Zhenyu Yang** *

* *Department of Energy Technology, Aalborg University, Esbjerg Campus, Niels Bohrs Vej 8, 6700 Esbjerg, Denmark, (e-mail: mvb, lha, dha, yang@et.aau.dk).*

Abstract:
The growing demand to optimize the deoiling performance for offshore oil & gas gives the incentive to improve existing control solutions by means of model-based control solutions. This paper proposes a separation efficiency grey-box model of a deoiling hydrocyclone. Grey-box modeling of deoiling hydrocyclones aims to combine knowledge from fluid dynamics with the data-driven parameter estimation to yield better accuracy than black-box derived models while keeping the computational load much lower than CFD-simulations. The model has to be reasonably accurate in all likely operating conditions and be computed in real-time, in order to be beneficial for advanced model-based control. The developed grey-box model is based on flow resistance and oil droplet trajectory analysis. The model functionally describes how the valve openings, inflow rates, and PDR set-points affect separation efficiency of the considered generic deoiling hydrocyclone. The results are reasonable and provide a fundamental overview of how the operational conditions affect separation efficiency. The model can be extended to account for changes in the axial velocity distribution, coalescence and breakup of droplets.

Keywords: Oil & Gas, Deoiling, Hydrocyclone, Separation Efficiency, Grey-Box Modeling

NOMENCLATURE

$[r, z]$	Radial and axial coordinate inside conical section.
$[v_r, v_z]$	Radial and axial velocity of oil droplet.
$[W, U, T]$	Axial, radial, and tangential velocity fields.
α	Imperfection penalty for V_i.
β	Cone angle.
$\Delta\rho$	Density difference between water and oil.
γ	Variable of integration for d.
$\hat{r}$	Normalized radius.
μ	Dynamic viscosity for water.
ϕ	Volume normalized droplet size distribution.
ρ	Density of oil-water mixture.
ε	Total volumetric separation efficiency.
a_z, b_z, c_z, d_z	Coefficients for $Y_z(\hat{r})$.
C	Virtual flow permeability constant.
d	Droplet diameter.
d_{100}	Smallest droplet diameter with 100% chance of being rejected.
F_s	Volumetric flow split.
$G(d)$	Grade efficiency.
L	Axial length of S_3
n	Forced/free vortex coefficient.
P	Absolute pressure.
PDR	Pressure drop ratio.
PT	Pressure transmitter.
Q	Volumetric flow rate.
Q_{scale}	Factor to scale axial velocity distribution to satisfy mass balance.
R	Radius.
S	Hydrocyclone element.
u	Control valve opening degree.
U_d	Slip speed between water and oil droplet.
V	Control valve.
$Y_z(\hat{r})$	Axial velocity distribution.

Subscripts

$_b$	Back pressure.
$_i$	Hydrocyclone inlet.
$_j$	Flow junction.
$_L$	Locus of zero axial velocity.
$_o$	Hydrocyclone overflow.
$_u$	Hydrocyclone underflow.
$_w$	Hydrocyclone wall.

1. INTRODUCTION

Deoiling hydrocyclones are applied in the offshore oil & gas industry for reducing the amount of oil content in the discharged produced water. The Danish Environmental Protection Agency (2016) defines an annual maximum total volumetric oil discharge of 202 tonnes for the Danish Sector of the North Sea. The OSPAR-Commission (2012) defines the maximum monthly average oil in water concentration of the discharged produced water into the North Sea as 30 parts per million. Well water production is increased during maturation of offshore operations, which renders the two limits a growing concern, thus promoting improvements that comply with the regulations for long-term oil and gas production (Yang et al. (2013)). The

choice of separation equipment used for cleaning of produced water varies based on factors such as produced water composition, cost-effectiveness, installation footprint, maintenance, and byproducts (Fakhrul-Razi et al. (2009)). As a result of many specialized technologies, multiple stages of separation equipment are often used (Fakhrul-Razi et al. (2009)). The main benefits of deoiling hydrocyclones are no moving parts, cost-effectiveness, small installation footprint, and scalability by coupling in parallel.

The configuration of a typical offshore deoiling hydrocyclone system is illustrated in Fig. 1, where PT_i, PT_u, and PT_o are inlet, underflow, and overflow pressure transmitters, respectively. Offshore installations have multiple liners connected in parallel to accommodate large production flow rates.

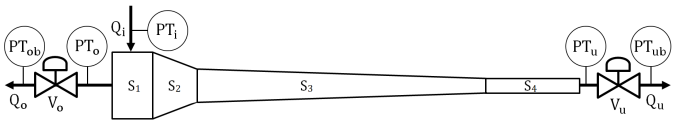

Fig. 1. Overview of single hydrocyclone liner and connected valves.

While the straightforward geometric design of the hydrocyclones combined with no moving parts is simple, the separation mechanisms depend on a wide range of interdependent flow conditions (Meldrum et al. (1987)). Due to a lack of cheap, reliable, and accurate measurements of the separation performance, PDR is used as control objective, as PDR serves as an intermediate indicator and is defined as

$$PDR = \frac{P_i - P_o}{P_i - P_u}. \tag{1}$$

Hydrocyclones are kept at a constant PDR during normal operating conditions. PDR is primarily chosen as control objective, as F_s is monotonically increasing with PDR within the entire valve operating range, where $F_s = Q_o/Q_u$ (Meldrum et al. (1987), Bram et al. (2017)).

In offshore process plants with many interconnected systems, some deployed control solutions can be contradictory, such as the three-phase separator water-oil interphase control and the PDR control of deoiling hydrocyclones (Yang et al. (2014)).

An incentive lies in the development of a dynamic mathematical model that reflects the separation performance and predicts the magnitude of performance gain or loss as a function of the input conditions. This enables tradeoffs to be defined at the operation that diverges from normal operation. For deoiling hydrocyclones, this tradeoff is low Q_o versus high ε. The insight that the grey-box modeling provides is also useful for cause-consequence and fault propagation analysis (Nielsen et al. (2017)).

This work combines a flow resistance model that predicts overflow and underflow flow rate, given the inlet and back pressures, with a separation efficiency model that statistically evaluate the oil droplet trajectories inside the hydrocyclone geometry. Section 2 describes the model functions, section 3 evaluates the model results, section 4 discusses the validation of the model, and section 5 provides concluding remarks.

2. EFFICIENCY MODEL STRUCTURE

This section combines the flow resistance model proposed by Bram et al. (2017) and a modified separation efficiency model proposed by Wolbert et al. (1995). The purpose of the combined model is to predict ε based on conventional pressure transmitters and feedback from control valves. The model has the inputs; $P_i, P_{ub}, P_{ob}, u_{V_u}, u_{V_o}$, and ρ, where ρ is considered a constant for this work. An overview of the combined model with all its sub-models can be seen in Fig. 2. The combined model has the following steps:

(1) Q_u and Q_o are calculated based on pressure drop over virtual orifices and control valves.
(2) Continuous phase water velocity fields (U, W, V) are solved based on flow, geometry, and continuity.
(3) Slip speed between droplet with specific size and water is calculated based on buoyancy and drag.
(4) The critical trajectory for the specific droplet size is calculated.
(5) $G(d)$ for the droplet with a specific size is calculated based on uniformly distributed start locations.
(6) Step 3 to 5 are repeated multiple times, each time with an increment in d, until $G(s) \geq 100\%$.
(7) The integrated product of $\phi_i(d)$ and $G(d)$ returns ε.

In order to estimate separation efficiency, a statistical estimation is formulated that evaluates the amount of oil droplet trajectories that leave through the overflow (rejected) and the underflow (passed). In order to evaluate these oil droplet trajectories within the hydrocyclone, the hydrocyclone geometry is decomposed into two cylindrical sections and two truncated cones. It should be noted that only the trajectories inside the hollow truncated cone S_3, as illustrated in Fig. 1, are evaluated in this work, as it is here the main part of the separation occurs according to Wolbert et al. (1995). Sections 2.1 to 2.6 describe the equations of the aforementioned steps.

2.1 Flow Resistance

The basic principle of the proposed flow resistance model is to estimate Q_u and Q_o given known upstream pressure P_i and downstream/back pressures P_{ob} and P_{ub}. This estimation is based on equations of pressure drop over flow resistances. The flow resistance of the hydrocyclone is decomposed into three internal virtual flow resistances; each with the flow permeability constants C_i, C_u, and C_u, where each of the virtual flow resistances share a common junction with the unknown pressure P_j. The pressure drops can be estimated as

$$P_i - P_j = \frac{(Q_u + Q_o)^2}{C_i}, \tag{2}$$

$$P_j - P_u = \frac{Q_u^2}{C_u}, \tag{3}$$

and

$$P_j - P_o = \frac{Q_o^2}{C_o}. \tag{4}$$

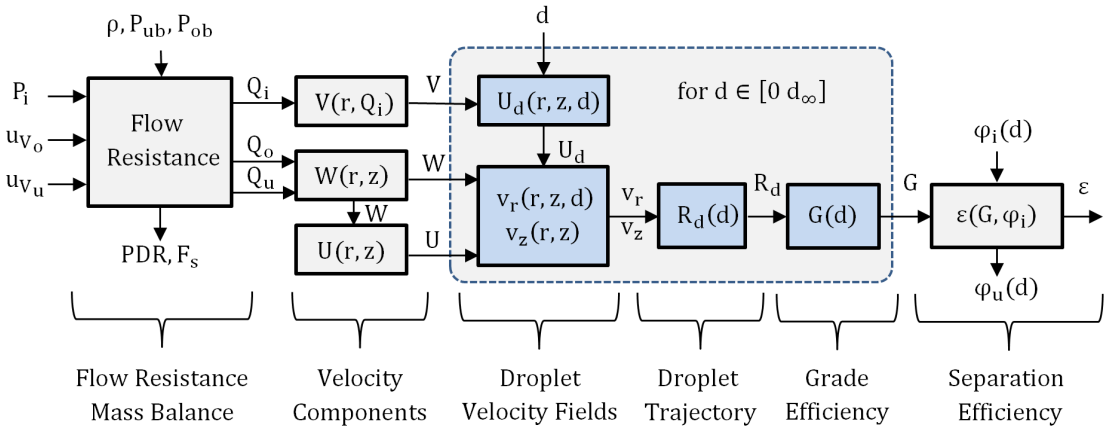

Fig. 2. Block diagram of efficiency model. Blue blocks are iteratively evaluated .

The pressure drop over the valves is dependent on the valves opening percentage. The pressure drop of V_o has been decomposed into two parts; one is u_{V_o}-dependent and the other one is similar to a fixed orifice. The valve decomposition was chosen as better suitability was observed. It is assumed that the decomposition is necessary due to the relatively small diameter of the overflow pipe i.e. that the V_o has a reduced orifice.

The pressure drop of the valves are considered as

$$P_u - P_{ub} = \frac{Q_u^2}{(C_{V_u} \cdot u_{V_u})^2} \tag{5}$$

and

$$P_o - P_{ob} = \left(\frac{Q_o}{C_{V_o 1} \cdot u_{V_o}^{\frac{1}{2}}} \right)^2 + \frac{Q_o^2}{C_{V_o 2}^2}. \tag{6}$$

Solving (2), (3), and (4) for PDR will return

$$\frac{P_i - P_o}{P_i - P_u} = \frac{C_u C_o Q_i^2 + C_u C_i Q_o^2}{C_u C_o Q_i^2 + C_o C_i Q_u^2}. \tag{7}$$

In a simplified case, where the inlet virtual flow resistor is neglected, (7) becomes

$$\frac{P_i - P_o}{P_i - P_u} = \frac{C_u Q_o^2}{C_o Q_u^2} \propto \frac{Q_o^2}{Q_u^2}, \tag{8}$$

thus resulting in PDR being proportional to F_s squared, which is a tendency that complies with Meldrum et al. (1987). The squared property derives from Q being squared in (2), (3), and (4). The proportionality constant between PDR and F_s^2 becomes C_u/C_o. The introduction of the inlet virtual resistor distorts this proportionality, but is necessary to let Q_u and Q_o be interdependent through (2). Equation (7) renders PDR to be monotonically increasing with F_s.

2.2 Tangental Velocity

Equations (2) to (6) solve the pressures; P_u, P_o, and P_j and the flows; Q_u and Q_o. With the geometry of S_3 defined, the tangential, axial, and radial velocity fields must be defined. Wolbert et al. (1995) describes how Q_i translates into tangential velocity at the inlet of the conical section by

$$v_i = \frac{4 \cdot \frac{Q_i}{2}}{\pi(0.35^2) \cdot (2 \cdot R_z(0))^2}. \tag{9}$$

The tangential velocity field inside the conical section can be described by

$$T(r) = \frac{\alpha \cdot v_i \cdot (2 \cdot R_z(0))^n}{r^n} \tag{10}$$

for two symmetrical inlets. It should be noted that $T(r)$ is time averaged and assumed to be axis-symmetrical (Dabir (1986)). Derksen and Van den Akker (2000) have shown that hydrocyclones can possess a proceeding vortex core, in which case the velocity fields are time dependent.

2.3 Axial Velocity

Ma (1993) uses a third degree polynomial

$$Y_z(\hat{r}) = a_z + b_z \cdot \hat{r} + c_z \cdot \hat{r}^2 + d_z \cdot \hat{r}^3 \tag{11}$$

to describe how the axial velocity is distributed as function of the normalized radius $\hat{r} = r/R_z(z)$. The radius of zero axial velocity satisfy

$$Y_z \left(\frac{R_L(z)}{R_z(z)} \right) = 0, \tag{12}$$

and Q_{scale} is introduced to satisfy mass balance through any axial cross section by

$$Q_u = \frac{2 \cdot Q_{scale}}{R_z(z)^2} \cdot \int_0^{R_z(z)} Y_z \cdot r \cdot dr. \tag{13}$$

With Y_z defined, $W(r, z)$ can be defined as

$$W(r, z) = Y_z \cdot \frac{Q_{scale}}{\pi \cdot R_z(z)^2}. \tag{14}$$

2.4 Radial Velocity

Firstly the continuous phase radial velocity is defined as

$$U(r, z) = \frac{-r}{R_z(z)} \cdot W(r, z) \cdot tan\left(\frac{\beta}{2}\right) \tag{15}$$

to account for the incline of the conical shape and to satisfy continuity (Kelsall (1952)). The radial velocity difference

between the dispersed and continuous phase is estimated by Stokes law

$$U_d(r) = \frac{\Delta\rho \cdot d^2 \cdot T(r)^2}{18 \cdot \mu \cdot r}, \tag{16}$$

which balances the drag and buoyancy forces on an oil droplet that is evaluated as a rigid sphere (Rajamani and Milin (1992)). Radial velocity expressed with Stokes law in (16) is only valid for creeping flow also called Stokes flow, where the droplet Reynolds number is lower than 1. Wolbert et al. (1995) states that droplets in liquid-liquid hydrocyclones are usually exposed to creeping flow.

2.5 Droplet Trajectory

As angular position of a droplet is not useful information for determining if it becomes rejected, only the radial and axial position of the droplet is used for trajectory evaluation. The radial and axial velocity of a droplet at (r, z) is defined as

$$\begin{bmatrix} v_r \\ v_z \end{bmatrix} = \begin{bmatrix} U(r,z) + U_d(r) \\ W(r,z) \end{bmatrix} \tag{17}$$

and produces a trajectory if the velocity updates the position iteratively. An illustration of a trajectory that crosses the two locations $(R_d, 0)$ and $(R_L(L), L)$ can be seen in Fig. 3.

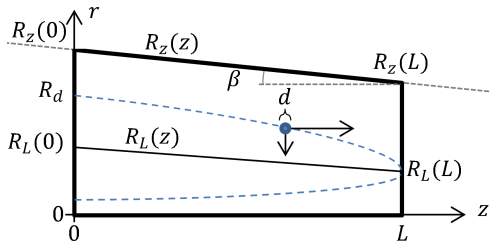

Fig. 3. Upper half cross section of S_3 with extreme case droplet trajectory for droplet with diameter d inside axis symmetric (r, z)-space.

When a droplet is moved inside R_L, its axial speed becomes negative as it is now moving towards the overflow and is considered rejected. A droplet that starts outside R_L, and never reaches R_L, is considered passed. Any start radii smaller than $R_d(d)$ would result in the droplet being rejected, and any larger start radii would result in the droplet entering the underflow. $R_d(d)$ is defined as the largest starting radius where a droplet with diameter d gets rejected and is solved iteratively by (17) starting at $(R_L(L), L)$ and stepping backwards in time. The iteration process starts at $d = 0$ increasing d each step until d_{100} is found as $G(d) = 1, \forall d \geq d_{100}$.

2.6 Efficiency Evaluation

The droplets are assumed to be uniformly distributed in the forward flow region between $R_L(0)$ and $R_z(0)$. With $R_d(d)$ defined, where $d \in [0, d_{100}]$, the grade efficiency is defined as

$$G(d) = \begin{cases} \dfrac{\pi \cdot R_d(d)^2 - \pi \cdot R_L(0)^2}{\pi \cdot R_z(0)^2 - \pi \cdot R_L(0)^2} & \text{if } d \leq d_{100} \\ 1 & \text{otherwise} \end{cases}, \tag{18}$$

which compares the total start area with the start area that results in the droplets being rejected.

To define ε, $\phi_i(d)$ must be known and volume normalized as smaller droplets contribute with smaller oil volumes per count. ε is solved as

$$\varepsilon = \int_0^\infty G(\gamma) \cdot \phi_i(\gamma) \cdot d\gamma \tag{19}$$

and due to the definition of $G(d)$ it can be divided into two terms resulting in

$$\varepsilon = \int_0^{d_{100}} G(\gamma) \cdot \phi_i(\gamma) \cdot d\gamma + \int_{d_{100}}^\infty \phi_i(\gamma) \cdot d\gamma, \tag{20}$$

using the variable of integration γ as a substitute for droplet diameter. This approach requires $\phi_i(d)$ to be known and solves $\phi_u(d)$ to be $G(d) \cdot \phi_i(d)$

3. MODEL EVALUATION

The combined model can be evaluated at various different conditions. To identify the relations between V_u, V_o, and ε the model is evaluated at 25-by-25 different valve combinations, where the opening degree range of the valves are $u_{V_u} \in [0.01, 0.99]$ and $u_{V_o} \in [0.01, 0.99]$. The simulation of the model is assumed under the following conditions:

- Vortex forced/free coefficient of n = 0.7.
- Imperfection penalty of $\alpha = 0.95$.
- a_z, b_z, c_z, and d_z of $-3.33, 12.0, -8.63$, and 1.19 respectively.
- $\phi_i(d)$ follows a log-normal distribution with mean $20\mu m$ and variance $0.0005\mu m^2$.
- Oil density of $950 kg/m^3$.
- Water density of $1000 kg/m^3$ and dynamic viscosity of 1.002 $mPa \cdot s$ (cP).
- All separation occurs in S_3.
- No droplet breakup or coalescence occur.
- Y_z is under the assumptions that F_s is below 10%.
- Y_z is independent of z, Q_o, and Q_i.
- A droplet is separated once its speed is negative in the axial direction.
- Droplets enters S_3 uniformly distributed in the flow that has a positive axial speed at $z = 0$.

Figure 4 shows ε at all points of the V_u-V_o-grid. The decrease in ε is significant when V_u is nearly closed. The only noticeable ε-change coursed by V_o is in the region where both valves are nearly closed. This indicates that V_u is far more dominant than V_o in case of manipulating ε in the entire operating region.

Figure 5 and 6 show Q_i, PDR, and ε generated by valve combinations of the grid. The color of the cells is an interpolated value between the cell's four corner point values. The black dots in Fig. 5 each indicate a specific V_u and V_o opening degree in the 25-by-25 grid. The black lines indicate a change in one of the valve openings. The

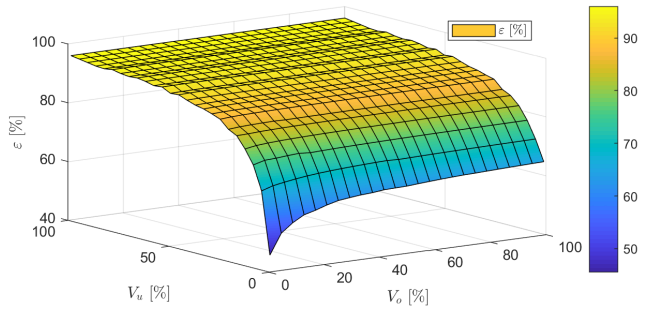

Fig. 4. Mapping of ε at all valve openings. Color indicates levels of ε.

nearly horizontal black lines follow changes of u_{V_o} and lines that appear to be exponentially decaying follow changes of u_{V_o}. The results presented in Fig. 5 show that u_{V_o} has an insignificant influence on Q_i and that u_{V_u} changes both Q_i and PDR based on operating point.

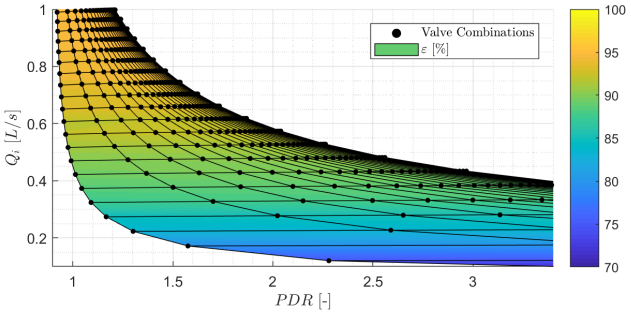

Fig. 5. Mapping of ε as function of PDR and Q_i at all valve openings. Color indicates levels of ε. Black dots are unique combinations of u_{V_u} and u_{V_o}. The black lines that connect the black dots indicate a change in u_{V_u} or u_{V_o}.

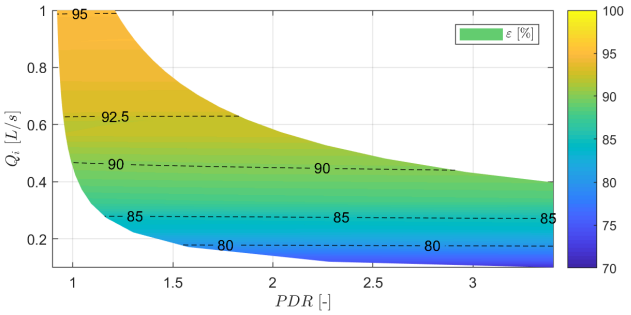

Fig. 6. Mapping of ε as function of PDR and Q_i at all valve openings with constant ε-contour dashed lines. Color indicates levels of ε.

Figure 5 and 6 show that ε is monotonically increasing with Q_i and insignificantly influenced by the PDR. It must be noted that the assumption of axial velocity distribution being independent of flow split produce model error, when diverging from the flow split that the axial distribution as designed for, which is for this case $F_s = 2\%$. It is shown in experimental cases that ε decrease significantly at very low PDR values (Meldrum et al. (1987)).

The horizontal black lines in Fig. 5 also show to what extent V_o can manipulate the PDR and that the opening degree of V_o has a marginal influence on Q_i. The exponential decaying black lines show how V_u affects both Q_i and PDR.

Figure 7 shows how PDR and F_s are related in the entire operating range. The dashed lines indicate constant F_s. The large inconsistent color change at low Q_i is a result of skewed quadrilateral cells.

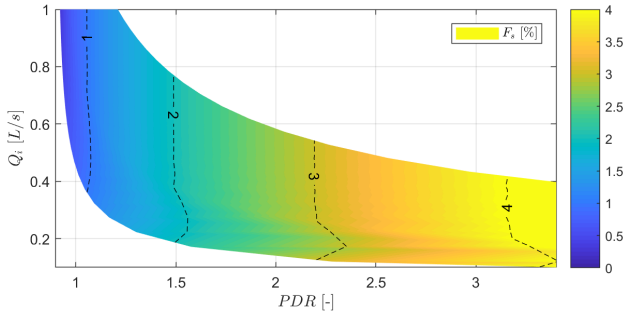

Fig. 7. Mapping of Flow split as function of PDR and Q_i at all valve openings. Color indicates levels of F_s. The dashed lines indicate 4 different F_s values

4. DISCUSSION

Each of the blocks in Fig. 2 contains equations of mechanics that should be validated. The difficulty of model validation range from comparing measurements of flow rate with the flow resistance model, to the grade efficiency that requires precise measurements of $\phi_i(d)$ and $\phi_u(d)$ which are known to be challenging (Yang (2011)).

The model predicts ε as a function of Q_i to be monotonically increasing. Meldrum et al. (1987) states that if Q_i is increased beyond a specific threshold, ε is prone to decrease as a result of increased shear forces. The model is unable to emulate this decrease without extension as droplet coalescence and breakup are not included. The test plant used by Bram et al. (2017) is limited by maximum P_i of 10bar which is insufficient for the hydrocyclone to exceed its threshold.

The model shows an insignificant correlation between PDR and ε, which is similar to what Meldrum et al. (1987) and Colman and Thew (1983) achieved. However, the experiments show that ε decreases to zero when V_o is closed. The model is unable to estimate this due to the constraints of Y_z, which are Q_o independent.

5. CONCLUSION

The virtual flow resistance model is able to estimate PDR and flow split to a satisfactory degree, and the combined model with trajectory analysis enables estimation of the separation efficiency of a deoiling hydrocyclone given geometric design, valve openings, pressures, and fluid properties. The virtual flow resistance equations have been proved to render PDR monotonically increasing with flow split. Modeling efficiency provides several benefits for developing or improving control solutions as the model can predict how much ε is compromised when diverging or

drifting between steady state operating points. This information is important when developing control algorithms for combined process systems, such as deoiling hydrocyclone coupled with an upstream three-phase separator. In addition, the model provides information on the influence of the overflow and underflow valve on the inlet flow and the separation efficiency at various operating conditions. Results show that the overflow valve has a marginal effect on the inlet flow rate and that the underflow valve changes both the inlet flow rate and PDR based on the operating point. The main computational load of the derived model is from computing a number of spacial trajectories depending on the desired resolution of the grade efficiency. As a result, the grade efficiency can be computed with good resolution in less than $1s$ on a standard office laptop using an Intel Core$^{\text{TM}}$ i7-5600 processor.

Future works for improving the model will focus on the model equations, as the model is inherently only valid under the assumptions defined in this paper. Specific assumptions could be redefined in a generalized way to increase accuracy at outer regions of the operating domain. An example of this is to redefine the axial velocity distribution to be dependent on the overflow flow rate, to account for the decrease in separation efficiency at the nearly closed region of the underflow valve. While the model structure is considered fixed, some model parameters are likely to change over time which gives the incentive to investigate if the model can be estimated online.

ACKNOWLEDGEMENTS

The authors thank the support from the DTU-DHRTC and AAU joint project - Grey-Box Modeling and Plantwide Control (AAU Pr-no: 878041). Thanks go to DTU colleagues: E. Bek-Pedersen, T. M. Jørgensen, and M. Lind. Thanks go to AAU colleagues: K. L. Jepsen, P. Durdevic, S. Pedersen, and S. Jespersen for many valuable discussions and technical support.

REFERENCES

Bram, M.V., Hansen, L., Hansen, D.S., and Yang, Z. (2017). Grey-box modeling of an offshore deoiling hydrocyclone system. In *Control Technology and Applications (CCTA), 2017 IEEE Conference on*, 94–98. IEEE.

Colman, D. and Thew, M. (1983). Correlation of separation results from light dispersion hydrocyclones. *Chemical Engineering Research and Design*, 61(4), 233–240.

Dabir, B. (1986). *Mean Velocity Measurements in a 3"-hydrocyclone Using Laser Doppler Anemometry*. University Microfilms.

Danish Environmental Protection Agency (2016). General authorization for Maersk Oil and Gas. Technical Report 1, Agency, Danish Environmental Protection.

Derksen, J. and Van den Akker, H. (2000). Simulation of vortex core precession in a reverse-flow cyclone. *AIChE Journal*, 46(7), 1317–1331.

Fakhrul-Razi, A., Pendashteh, A., Abdullah, L.C., Biak, D.R.A., Madaeni, S.S., and Abidin, Z.Z. (2009). Review of technologies for oil and gas produced water treatment. *Journal of hazardous materials*, 170(2), 530–551.

Kelsall, D. (1952). A study of the motion of solid particles in a hydraulic cyclone. Technical report, Atomic Energy Research Establishment, Harwell, Berks (England).

Ma, B.F. (1993). *Epuration des eaux résiduaires de l'industrie pétrolière par hydrocyclonage: Mise au point d'un nouveau hydrocyclone triphasique*. Phd thesis, Toulouse, INSA.

Meldrum, N. et al. (1987). Hydrocyclones: A solution to produced water treatment. In *Offshore Technology Conference*, volume 3, 669–76. Offshore Technology Conference.

Nielsen, E.K., Bram, M.V., Frutiger, J., Sin, G., and Lind, M. (2017). Modelling and validating a deoiling hydrocyclone for fault diagnosis using multilevel flow modeling. In *International Symposium on Future Instrumentation & Control for Nuclear Power Plants*.

OSPAR-Commission (2012). *North Sea Manual on Maritime Oil Pollution Offences*. OSPAR, London.

Rajamani, R.K. and Milin, L. (1992). Fluid-flow model of the hydrocyclone for concentrated slurry classification. In *Hydrocyclones*, 95–108. Springer.

Wolbert, D., Ma, B.F., Aurelle, Y., and Seureau, J. (1995). Efficiency estimation of liquid-liquid hydrocyclones using trajectory analysis. *AIChE Journal*, 41(6), 1395–1402.

Yang, M. (2011). Measurement of oil in produced water. In *Produced water*, 57–88. Springer.

Yang, Z., Pedersen, S., and Durdevic, P. (2014). Cleaning the produced water in offshore oil production by using plant-wide optimal control strategy. In *2014 Oceans-St. John's*, 1–10. IEEE.

Yang, Z., Stigkær, J.P., and Løhndorf, B. (2013). Plantwide control for better de-oiling of produced water in offshore oil & gas production. *IFAC Proceedings Volumes*, 46(20), 45–50.